Separation and Purification Technology 341 (2024) 126720

Contents lists available at ScienceDirect

Separation and Purification Technology

journal homepage: www.elsevier.com/locate/seppur

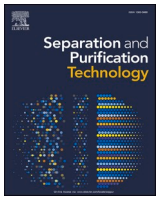

Amine-grafted on boron modified SBA-15 for direct air capture of CO_2

Hao Yuan [a], Peng Li [a,b], Xiali Sun [a], Dingli Cen [c], Decun Luo [a], Xianghui Yan [b], Guangping Lei [c], Wentao Zheng [d], Zhun Hu [a,*], Ralph T. Yang [e,*]

[a] Institute of Industrial Catalysis, School of Chemical Engineering and Technology, Xi'an Jiaotong University, Xi'an Shaanxi 710049, China
[b] School of Materials Science and Engineering, North Minzu University, Yinchuan 750021, China
[c] School of Energy and Power Engineering, North University of China, Taiyuan 030051, China
[d] State Key Laboratory of Coal Conversion, Institute of Coal Chemistry, Chinese Academy of Sciences, Taiyuan 030001, China
[e] Department of Chemical Engineering, University of Michigan, Ann Arbor, MI, USA

ARTICLE INFO

Keywords:
Direct air capture
Boron doped SBA-15
Amine grafted
In situ-DRIFTS

ABSTRACT

Amine loading was considered to be the main factor affecting the CO_2 capture performance of amine-grafted mesoporous materials. In this study, SBA-15 with varied boron loadings was investigated to understand the effect of amine loading on the CO_2 adsorption ability. It was found that the dynamic CO_2 capacity with respect to boron loading showed a volcano curve. Proper boron additives with acid treatment could improve the amount of silanol in SBA-15. Temperature programmed desorption results indicated that the dynamic CO_2 capacity was in linear relationship with the amine loading, which was decided by silanol via its reaction with graft amines. Moreover, amine grafted SBA-15 with boron additive showed good cyclic stability and vapor resistance. *In situ*-DRIFTS showed that surface silanol groups participate in the CO_2 capture process by forming carbamic acid (hydrogen-bonded) and silylpropylcarbamate. These results provide a quantitation understanding between dynamic CO_2 capacity, amine loading and hydroxyl groups, which would provide a guideline for the development of high dynamic CO_2 capacity in the direct air capture.

1. Introduction

Climate change caused by CO_2 emissions has brought serious environmental problems [1]. Research and development of carbon capture utilization and storage (CCUS) technology to reduce emissions is the future development trend. The key to CCUS technology is how to achieve large-scale, low-cost CO_2 capture. At present, the research on CO_2 capture technology has expanded from the traditional capture of point sources (e.g., power plants, industrial production) to the use of biomass (Biomass energy carbon capture and storage, BECCUS) or adsorbents (Direct air carbon capture, DAC) to capture CO_2 directly from the atmosphere. Among these technologies, DAC technology has the advantages of simple process, small corrosion to equipment, low consumption of resources (land, energy, etc.), and wide application occasions, becoming a popular direction in the field of CO_2 adsorption and separation. DAC technology is complementary to traditional capture technology and can reduce the risk and pressure of achieving net zero emissions in traditional industries while also expanding applications [2,3].

The main types of DAC adsorbents due to activated carbon, zeolites, mesoporous silicates, metal–organic framework materials (MOFs), moisture wetting adsorbents, and amine-modified adsorbents [3–5]. DAC adsorbents mainly evaluated the materials from the aspects of capture capacity, adsorption and desorption temperature, adsorption kinetic mechanics, and reusability. Capturing CO_2 using alkali solution or alkali metal oxide absorbent is simple to implement. At an earlier stage, DAC projects [6,7] mainly focused on the alkali solution or alkali metal oxide absorbent, due to strong CO_2 capture capacity. However, this technical route possessed high energy consumption and loss of capacity after cycles of carbonation/decarbonation [8,9], this limited its widespread application. Much attention was paid on the development of zeolites and carbon materials for CO_2 adsorption [10,11]. Zeolites and carbon materials showed lower regeneration temperatures. However, these materials lacked adsorption selectivity, which was greatly affected by water vapor content [12–14]. The development of adsorbent materials with excellent performance and high vapor resistance was the key to the DAC technology.

The modification for mesoporous silica (e.g., SBA-15, MCM-41) has

* Corresponding authors.
E-mail addresses: huzhun@mail.xjtu.edu.cn (Z. Hu), yang@umich.edu (R.T. Yang).

https://doi.org/10.1016/j.seppur.2024.126720
Received 14 November 2023; Received in revised form 25 January 2024; Accepted 5 February 2024
Available online 15 February 2024

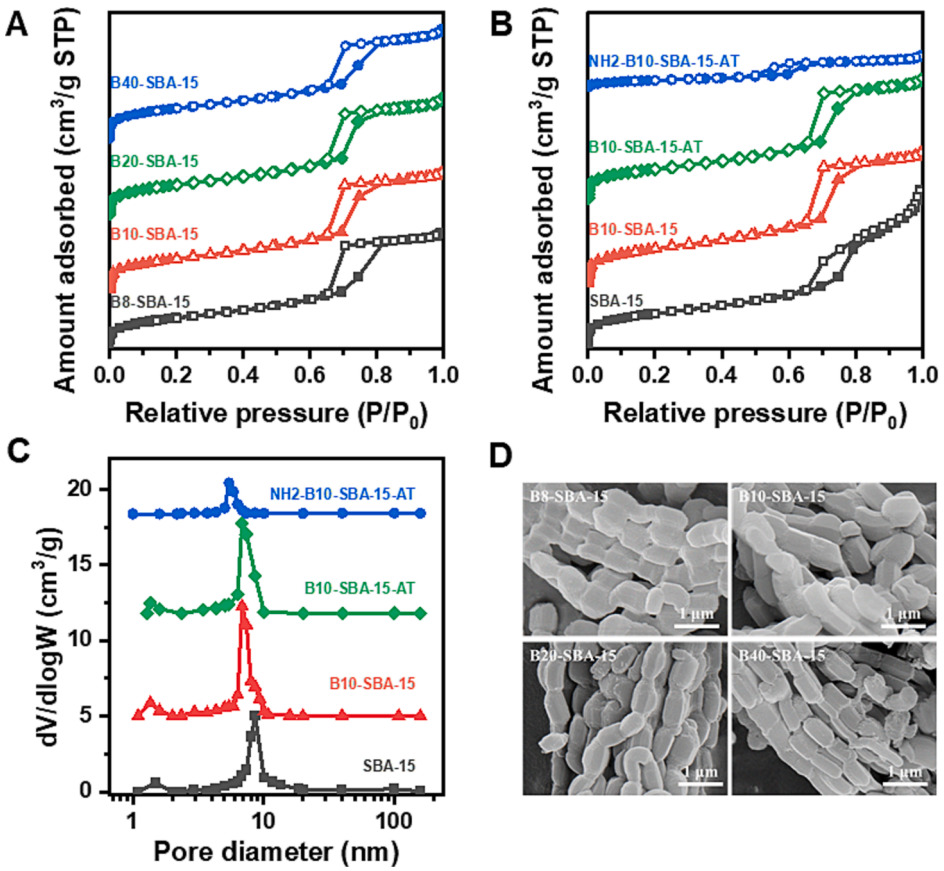

Fig. 1. A: N_2 adsorption–desorption isotherms of B8-SBA-15(■), B10-SBA-15(▲), B20-SBA-15(◆); B40-SBA-15(●); B: N_2 adsorption–desorption isotherms of SBA-15 (■), B10-SBA-15(▲), B10-SBA-15-AT(◆) and NH2-B10-SBA-15-AT(●); C: BJH pore size distributions. D: SEM images of BX-SBA-15.

Table 1
Physicochemical properties of SBA-15 and NH2-BX-SBA-15-AT samples.

Sample	S_{BET} (m^2/g) [a]	V_{total} (cm^3/g) [b]	Pore size (nm) [c]
SBA-15	649	1.31	9.4
NH2-SBA-15	187	0.53	10.2
B8-SBA-15	660	1.06	7.0
B10-SBA-15	669	1.07	6.8
B20-SBA-15	643	1.06	6.8
B40-SBA-15	654	1.00	7.0
B8-SBA-15-AT	452	0.98	7.4
B10-SBA-15-AT	587	0.99	7.1
B20-SBA-15-AT	595	1.01	7.1
B40-SBA-15-AT	597	0.97	7.2
NH2-B8-SBA-15-AT	212	0.39	6.4
NH2-B10-SBA-15-AT	148	0.26	6.2
NH2-B20-SBA-15-AT	207	0.39	6.6
NH2-B40-SBA-15-AT	211	0.40	6.7

[a] BET surface area calculated from the adsorption branch;
[b] Pore volume estimated from the single-point amount adsorbed at P/P0 = 0.99;
[c] Determined from the maximum of BJH pore size distribution.

been regarded as a promising way for the adsorbed materials with high CO_2 capacity and vapor-resistance [15–17]. Amine-functionalized mesoporous silica materials have great potential for DAC due to their high tolerance to water and temperature, low regeneration energy consumption, good reusability [14,16,18]. The amination of materials is achieved through physical impregnation or chemical grafting. In the impregnation method, amine materials were usually dispersed by organic solvents and loaded into the pores of mesoporous silica. This method can achieve higher amine loading and usually had a larger capture capacity. However, the interaction between the impregnated amine and the surface of the material was weak, the amino group easily falls off during capture, resulting in poor cycle stability. In addition, the disorderly stacking of amines also leaded to low utilization level of amino groups (Table S1). In order to solve these problems, the researchers developed a chemical grafting method by the silanization reaction of aminosilane and hydroxyl of mesoporous silica. Amine loading was considered to be the main factor determining the adsorption performance of modified materials. Therefore, increasing the surface silanol density of mesoporous silica is a direct way to increase the amine loadings.

The silanol groups on the surface of ordered mesoporous silica are mainly formed by the process of silica network polymerization [19]. The silanol groups could be changed via the modification of preparation method and after-treatment method. The template was usually removed by calcination and the high temperature of this process will reduce the number of silanol groups on the surface [20]. Therefore, a method to retain more surface silanol is to develop mild template removal methods, such as solvent extraction [21]、microwave assisted extraction [22] and ultrasonic treatment [23]. Another way is to recover silanol groups via rehydroxylation of calcined mesoporous silica. Norton et al. [24] discovered the reversible formation of silanol groups in two-dimensional siliceous nanomaterials, a similar regeneration method was also found in the SBA-15 [25]. Adjusting the material structure is also a feasible path. The introduction of heteroatoms in the preparation of silica composite adsorbents could altering the acid/base properties [26,27] and thus enhance CO_2 adsorption capacity [28]. The density of surface silicon groups was increased by incorporating heteroatoms into the silica network. Moreover, previous work[29] increased the silanol group via removing heteroatoms by acid treatment to create defects (silicon hydroxyl nests) composed of four silicon hydroxyl groups, which significantly improved the density of silicon hydroxyl groups and CO_2

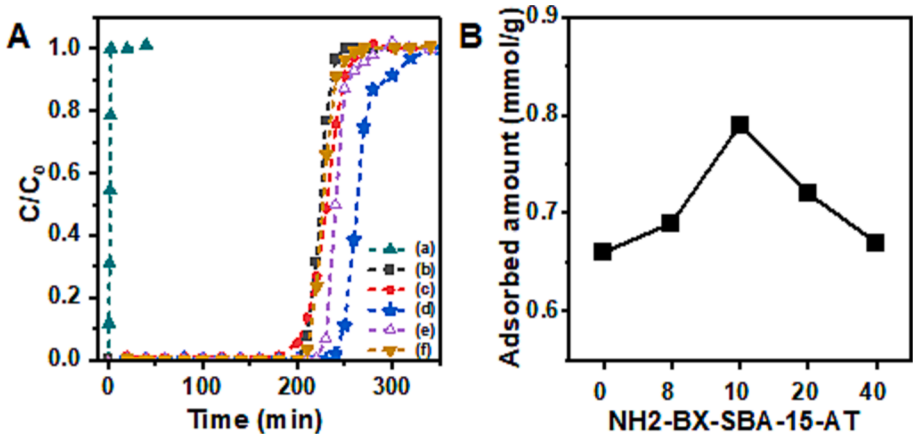

Fig. 2. A: CO_2 breakthrough curves of (a) SBA-15 (▲), (b) NH2-SBA-15 (■), (c) NH2-B8-SBA-15-AT (●), (d) NH2-B10-SBA-15-AT (★), (e) NH2-B20-SBA-15-AT (△), (f) NH2-B40-SBA-15-AT (▼) under dry 400 ppm CO_2 flow feed at 25 °C; B: The adsorbed amount of NH2-BX-SBA-15-AT (X = 0, NH2-SBA-15).

Table 2
Amount adsorbed, desorption peak temperature, silanol amount and amine loadings.

Samples	Amount adsorbed (mmol/g)	Desorption peak temperature (°C)	Silanol amount (a.u.) [a]	Amine loadings (a.u.)
NH2-B8-SBA-15-AT	0.69	101	6.23	5.98
NH2-B10-SBA-15-AT	0.79	105	7.34	8.63
NH2-B20-SBA-15-AT	0.72	95	4.91	6.63
NH2-B40-SBA-15-AT	0.67	107	4.61	6.09

[a] Silanol amount refers to the content before amine grafted.

capacity. Compared with the material prepared by the traditional process, the adsorption capacity (under 410 ppm CO_2) of the material is increased by three times. The method of using skeleton doping and re-removal may be an effective way to increase the density of silicon hydroxyl groups.

In this study, SBA-15 materials with different boron content were synthesized and the heteroatoms were removed by acid treatment. N_2 adsorption and temperature programmed desorption characterized the silanol and amine loading of SBA-15 based materials. Further, *in situ*-DRIFTS was used to understand the CO_2 adsorption pathway.

2. Experiment section

2.1. Syntheses of SBA-15

The mesoporous silica SBA-15 was synthesized based on previously reported methods [29–31]. The molar composition of final mixture was TEOS / P123 / HCl / H_2O = 0.82: 0.0138: 4.75: 138.9. In a typical synthesis, 4 g of P123 ($EO_{20}PO_{70}EO_{20}$) was added to 125 mL of 1.9 M HCl and stirred 2 h. The solution was hated to 40 °C, and 9.1 mL of tetraethyl orthosilicate (TEOS) was added dropwise and stirred for 24 h. Next, the mixture was transferred to a Teflon autoclave and aged at 110 °C for 24 h. The resulting solid was filtered and washed with DI water. The collected white sample was dried overnight and subsequent calcined at 2 °C/min to 550 °C under an air flow to remove the template P123. The sample was designated as SBA-15.

2.2. Boron doped SBA-15

Boron doped SBA-15 was synthesized using the hydrothermal methods reported by R. van Grieken et al [26,27]. Boric acid was used as boron source. The solution was heated up to 40 °C before boron source was added. Then, solid boric acid was added, the mixture was stirred at 40 °C for 20 h, other steps were consistent with the synthesis of SBA-15. The obtained samples were denoted as BX-SBA-15, where X was Si/B

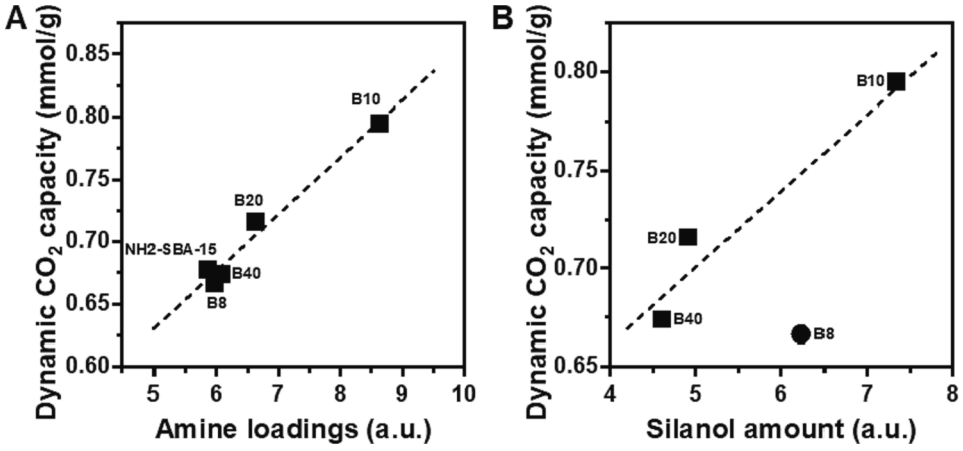

Fig. 3. The relationship between the adsorbed amount and A:silanol amount, B: amine loadings.

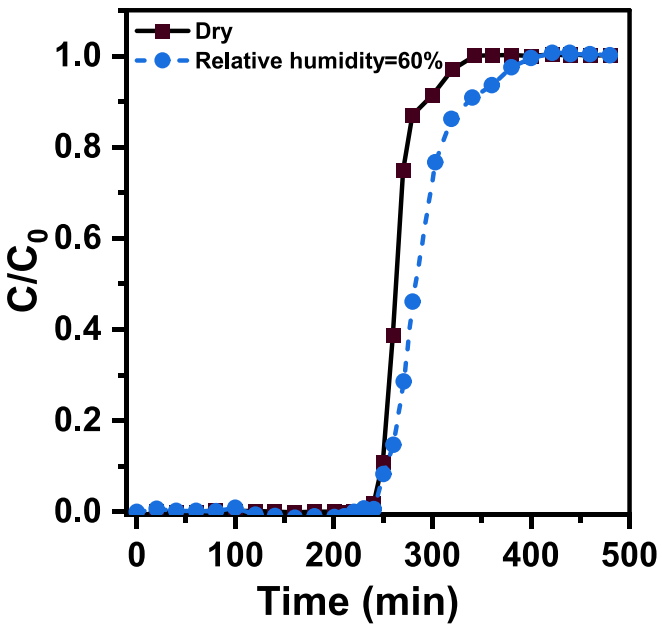

Fig. 4. CO_2 breakthrough curves of NH2-B10-SBA-15-AT under dry (■) and wet (●) 400 ppm CO_2(balanced in Ar) flow at 25 °C. Relative humidity (R.H) for wet condition is 60 %.

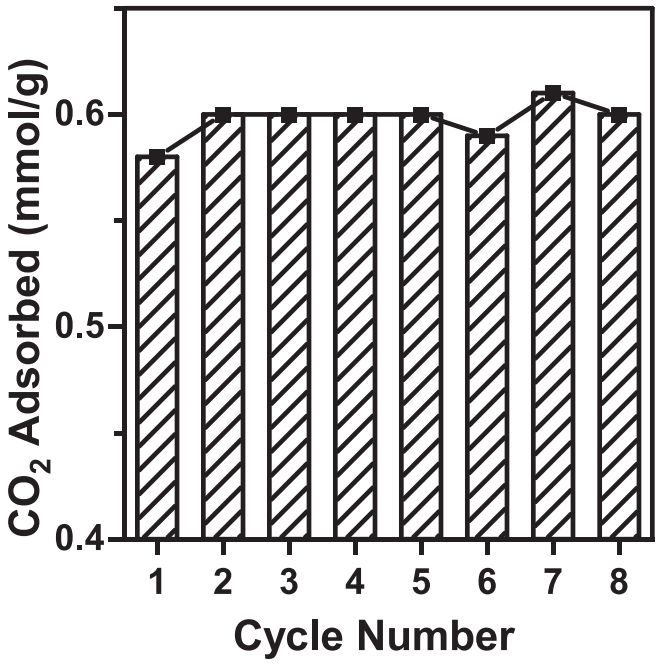

Fig. 5. Cyclic stability studies for NH2-B10-SBA-15-AT at 25 °C adsorption in dry 400 ppm CO_2 flow (balanced in Ar) and 105 °C desorption in N_2 flow.

nominal molar ratio (X = 8, 10, 20, 40).

2.3. Acid treatment

Acid treatment was aim to remove boron in the BX-SBA-15. Typically, 2 g of BX-SBA-15 and 1.9 g of citric acid were added to 100 mL of 1.9 M HCl solution. The mixture was refluxed at 80 °C for 8 h and then washed thoroughly with DI water. The solid was collected by filtration and dried at 120 °C for 12 h. The sample obtained after acid treatment was designated as BX-SBA-15-AT.

2.4. Amine grafting

The amine grafting process was performed following previously reported methods [16,29]. All supports were dried at 100 °C for at least 12 h prior to amine grafting. Typically, 1 g of support materials was mixed with 100 mL of anhydrous toluene. The mixture was stirred at room temperature for 10 min. Then, 10 mL of 3-aminopropyl trimethoxysilane (APTMS) was added to the mixture slowly. The mixture was stirred and refluxed at 80 °C for 12 h. The amine grafted samples were filtered and washed with copious amounts of toluene, then dried at 50 °C. The amine grafting procedures were performed on SBA-15 and BX-SBA-15-AT. The resulting materials were designated as NH2-SBA-15 and NH2-BX-SBA-15-AT respectively.

2.5. Characterization

N_2 adsorption/desorption isotherms were obtained at −196 °C by Micromeritics ASAP 2460 Analyzer. Before each test, materials were degassed at 105 °C for 12 h.

The content of boron doped within the skeleton of the material was determined by Inductively Coupled Plasma Optical Emission Spectrometer (ICP-OES, Agilent 5110). The relative content of silicon hydroxyl and amine groups on the surface of the material was measured by temperature programmed desorption experiment. The sample was first pretreated for 2 h at 120 °C in a flowing Ar, then heated to 800 °C at a rate of 10 °C/min for 30 min. In this process, the effluent gas was monitored by the mass spectrometry (Altamira Instruments, Master 400). Amino and silicon hydroxyl group were detected by the mass-charge ratio of 15 and 18, respectively.

Dynamic adsorption capacity was measured in a vertical fixed-bed reactor at 25 °C under 400 ppm CO_2 (balance with Ar) at gas-hourly space velocity (GHSV) of 10000 h^{-1}. The outlet gas was detected by mass spectrometry. Samples were pressed and sieved for a size range of 40–60 mesh. Before each adsorption measurement, the fixed bed was pretreated at 105 °C for 2 h under a flow of N_2. When the CO_2 signal reaches 400 ppm and is stable for 30 min, the breakthrough test ends. Cyclic test use was measured in the same experimental operation.

In situ-DRIFTS was carried out on a Nicolet iS50 apparatus in the range of 650–4000 cm^{-1}. The temperature was controlled using a temperature control instrument. The mass flow controllers were used to manipulate the gas composition. The details of *in situ*-DRIFTS were carried out with the following sequences: (i) pretreatment at 105 °C under 20 mL/min N_2 flow, (ii) adsorption of 400 ppm CO_2 at 25 °C.

3. Result and discussion

3.1. Physicochemical properties of the adsorbents

The N_2 adsorption–desorption isotherms and the Barrett-Joyner-Halenda (BJH) pore size distributions of the samples are shown in Fig. 1A, 1B and 1C. All the samples exhibited IV (a) type isothermal behavior and H1 type hysteresis loop, which correspond to mesoporous materials according to the classification criteria of IUPAC [32]. The partial pressure and shape of hysteresis loop were related to the pore structure and pore network properties. The mesoporous structure of SBA-15 was affected by boron doping and removal. The details of the results for the samples are shown in Table 1. The average pore size of B10-SBA-15, B10-SBA-15-AT and NH2-B10-SBA-15-AT was 6.8, 7.1 nm and 6.2 nm, smaller than SBA-15 (9.4 nm). With the doping and removal of boron source, both the pore size and pore volume were lower than those of SBA-15, a finding similar to that reported in previous literature [27,29].

For the sample with acid treatment, compared with BX-SBA-15, the BET surface area of BX-SBA-15-AT decreased and the pore size increased slightly, which may be caused by the collapse or expansion of some pores caused by the removal of boron atoms. After chemical amine

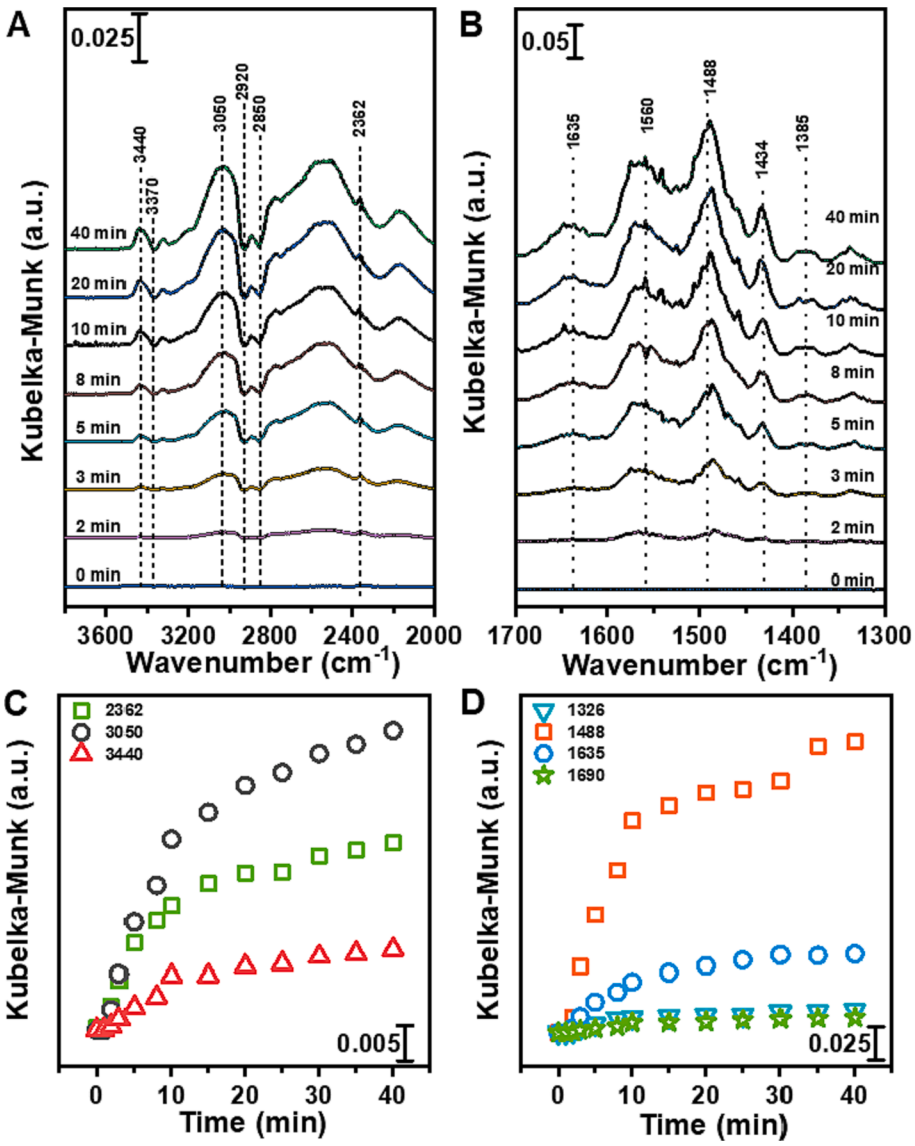

Fig. 6. FTIR spectra of NH2-B10-SBA-15-AT adsorption and desorption process.

grafting, the BET surface area and pore size of the material decreased significantly due to the amine group occupying the pores. In addition, it was also observed that the micropores and small mesopores caused by the embedding of the EO group on the P123 chain of the template agent into the silica skeleton had obvious peaks in the pore size distribution of SBA-15 and B10-SBA-15, and disappeared after amine modification. These disordered tunnels connecting the main channel will not appear in XRD, however nitrogen adsorption and desorption can be measured. The similar results were also observed in the previously results [33,34]. The texture characteristics of BX-SBA-15 indicated that boron doping can significantly affect the structural parameters of SBA-15. Combined with the N_2 adsorption–desorption isotherms, it can be clearly seen that both boron doping and acid treatment did not alter the ordered structure of SBA-15 materials.

Fig. 1D shows the scanning electron microscope (SEM) images of BX-SBA-15. The original SBA-15(Figure S1) owned a broken short rod shape, which is similar to the previous reports [35–37]. The short rod structure of boron-doped materials was similar to extending the hydrothermal time, due to the acidity being one of the main factors affecting the synthesis of SBA-15 [38], the change in the acidity of the synthesis system caused by adding different boric acid during preparation may be the reason for this phenomenon. The small-angle XRD patterns of SBA-15 and B10-SBA-15 were presented in Figure S1. The diffraction peaks at (1 0 0), (1 1 0), and (2 0 0) of the typical hexagonal cell can be clearly distinguished in the patterns. The Miller index hkl, with l = 0 for all diffraction peaks, is a typical feature of the two-dimensional hexagonal structure of SBA-15 as reported in references [30,39,40].

3.2. CO_2 capture performance

Fig. 2A shows the breakthrough curve of NH2-SBA-15 and NH2-BX-SBA-15-AT samples. All the NH2-BX-SBA-15-AT showed higher CO_2 adsorption capacity than NH2-SBA-15. All the breakthrough curves showed an “S” type, which was a compensation effect between CO_2 diffusion and adsorption rate. At the beginning of adsorption, the material does not adsorb CO_2 on the surface and has the most amino active sites. At this stage, adsorption is most likely to occur, and the adsorption rate is high. As adsorption proceeded, the amino active sites were gradually occupied. The corresponding quantification results are shown in Table 2.

The dynamic CO_2 adsorption capacities of NH2-B8-SBA-15-AT, NH2-B10-SBA-15-AT, NH2-B20-SBA-15-AT and NH2-B40-SBA-15-AT were 0.69 mmol/g, 0.79 mmol/g, 0.72 mmol/g and 0.67 mmol/g,

Table 3
Assignment of the IR bands.

Frequency (cm^{-1})	Assignation	Species	References
1434	COO^- sym stretching	ammonium carbamate ion pairs	[46]
1488	COO^- stretching	carbamate	[52,53]
1525	NH deformation + C-N stretching	silylpropylcarbamate carbamic acid (hydrogen-bonded; not resolved)	[46]
1560|	COO^- asym stretching	ammonium carbamate ion pairs	[46,50]
1650–1635	NH_3^+ deformation	ammonium carbamate ion pairs	[46,47]
1700–1680	C = O stretching	carbamic acid (hydrogen-bonded)	[48,50]
1715	C = O stretching	silylpropylcarbamate (hydrogen-bonded)	[46,49]
2362	CO_2 asym stretching,	physiosorbed linear CO_2	[49,54]
3050	N–H stretching vibration	NH_3^+	[55]
3300	NH_2 sym stretching	primary amine (R-NH_2, R: alkyl)	[46,47]
3300——3360	N–H stretch	$–NHCOO^-$	[47]
3370	NH_2 asym stretching	primary amine (R-NH_2, R: alkyl)	[46,47]
3440	N–H stretching	ammonium carbamate ion pairs, carbamic acid (hydrogen-bonded)	[47,48,54]

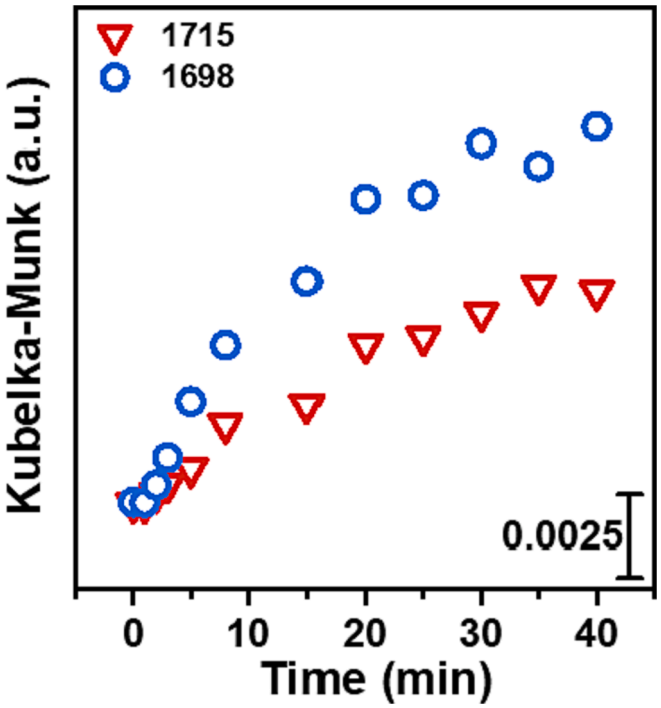

Fig. 7. The signal changes of silylpropylcarbamate (1715 cm^{-1}) and carbamic acid (hydrogen-bonded, 1698 cm^{-1}) during the adsorption.

respectively. The dynamic CO_2 capacity with respect to boron loading of NH2-BX-SBA-15 was displayed in Fig. 2B. The adsorption capacities of NH2-BX-SBA-15-AT increased with the increase in the Si/B ratio from 8 to 10, and then decreased with further increase from 10 to 40. The adsorption capacity of NH2-BX-SBA-15-AT showed a volcano curve with Si/B ratio, maximum at 10. When CO_2 was adsorbed on amine-functionalized silica adsorbents, the contribution of chemisorption to the material's adsorption capacity was much higher than that of physical adsorption [41]. This means that amine loading plays an important role in determining the CO_2 adsorption capacity. In order to understand the effect of boron loading on the dynamic CO_2 capacity on the NH2-BX-SBA-15-AT, the amount of amine loading and hydroxyl groups were further investigated.

The amount of amine and hydroxyl groups on the surface of the material was measured by TPD process with MS detection. The weight loss process of silicon hydroxyl was mainly divided into two stages [42,43]: (a) the weight loss below 150 °C was caused by the water and gas adsorbed by the material; (b) weight loss above 150 °C was attributed to dehydroxylation by condensation of silanol groups. According to the results of MS, we obtained the amounts of silicon hydroxyl content and amine loading, the results are shown in Table 2. A linear relationship between dynamic CO_2 capacity and amine loading was observed (Fig. 3A), indicating that the CO_2 capacity was decided by the amine loadings. The NH2-B10-SBA-15-AT sample with the highest amine loading sample showed the best adsorption capacity.

Fig. 3B shows the relationship between hydroxyl groups and dynamic CO_2 capacity. By measuring the water content generated by the decomposition of BX-SBA-15-AT in TPD test, the number of silanol groups can be determined. More silanol can provide the more sites for amine grafting. A linear relationship between silanol and dynamic CO_2 capacity was observed among Si/B ratios ranging from 10 to 40, indicating that the dynamic CO_2 capacity was determined by silanol content. All these results indicate that dynamic CO_2 capacity is determined by amine loading, which is dependent on hydroxyl groups.

Fig. 4 shows the CO_2 breakthrough curves of NH2-B10-SBA-15-AT under dry and wet. The dynamic CO_2 capacities were 0.79 mmol/g and 0.88 mmol/g under dry and wet conditions, respectively. The difference was mainly ascribed to the existence of extra hydroxyl groups. Under dry conditions, two amine groups are required to adsorb a CO_2 molecule, while under wet conditions, water molecules will cooperate with a single amine group to capture CO_2 [44,45]. This cooperation improves the utilization efficiency of amine groups and thus the adsorption capacity of the material. Obviously, NH2-B10-SBA-15-AT exhibits high CO_2 adsorption performance at low CO_2 concentrations under both dry and wet conditions.

An industrial adsorbent should own excellent regeneration performance and cycle stability. Fig. 5 shows continuous absorption and desorption stability of NH2-B10-SBA-15-AT was tested at 25 °C, 400 ppm CO_2. After each adsorption, the material was regenerated at 105 °C, in N_2. The NH2-B10-SBA-15-AT sample showed excellent adsorption performance after seven cycles. All these results indicated that the grafted groups in the material not only enhanced the CO_2 capacity, but also exhibited good cyclic regeneration ability.

3.3. *In situ-DRIFTS of the adsorption process*

To provide molecular level insight into the adsorption process of CO_2 on the material, *in situ*-DRIFTS experiments were carried out. Fig. 6 shows the infrared spectra of adsorbed species with respect to time on NH2-B10-SBA-15-AT during the process of absorption. (See Table 3 for a representation of the species formed.) The background spectrum in the experiment was collected after 2 h pretreatment using NH2-B8-SBA-15-AT under N_2 to avoid the interference of adsorption species under atmosphere environment.

Organic amines rapidly react with dry CO_2, forming ammonium carbamate ion pairs [46]. The band at 2362 cm^{-1} is attributed to the linear physical adsorption of CO_2. Peaks at 3440 cm^{-1} and bands in the range of 3300–3360 cm^{-1} correspond to N–H vibrations within the ammonium carbamate ion pairs. The peaks at 1560 cm^{-1} and 1433 cm^{-1} were assigned to the asymmetric and symmetric stretching vibrations of COO^- in the ammonium carbamate ion pairs [46,47]. Negative peaks at 3300 cm^{-1} and 3370 cm^{-1} indicated the asymmetric stretching vibration and symmetric stretching vibration of the NH_2 group in the

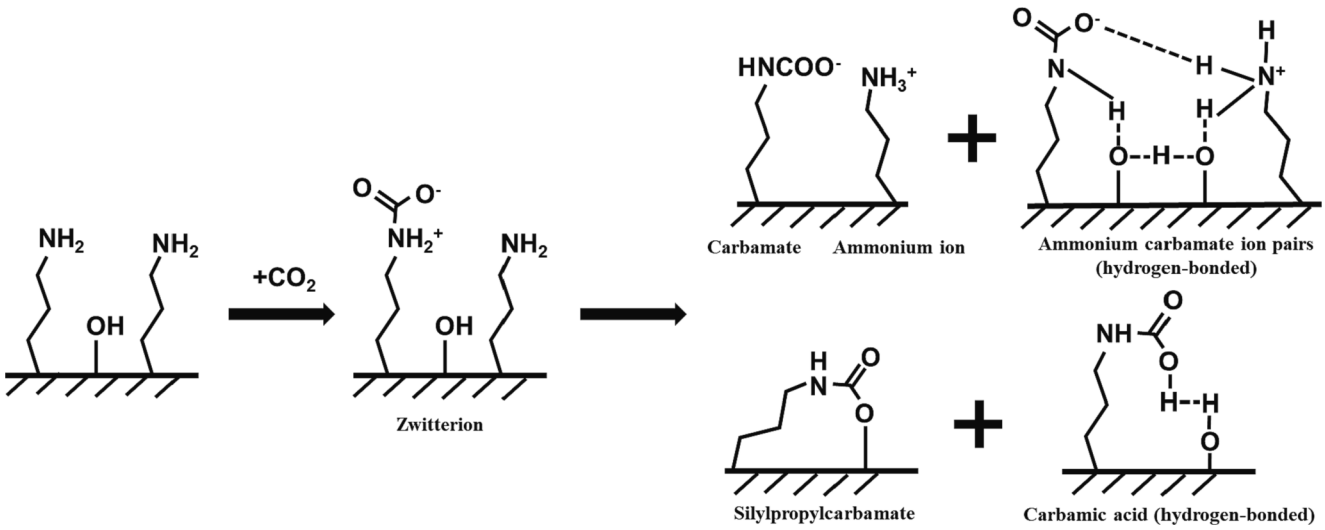

Fig. 8. Mechanism for the reaction of CO_2 under dry condition.

hydrogen-bonded amino group, confirming the involvement of the hydrogen-bonded amino group in the CO_2 adsorption process [47]. Peaks at 1700–1680 cm^{-1} and 1715–1710 cm^{-1} were associated with carbamic acid (hydrogen-bonded) [48] and silylpropylcarbamate [46,49]. Fig. 7 illustrates the signal changes of the two aforementioned adsorbed species, suggesting the simultaneous presence of both, with a higher quantity of hydrogen-bonded carbamic acid compared to silylpropylcarbamate.

Fig. 6 illustrates the introduction of CO_2, where bands at 2362 cm^{-1} (indicative of physically adsorbed CO_2) and 3050 cm^{-1} (associated with ammonium ion) were initially detected. As the adsorption time increased, the intensity of bands at 1560 cm^{-1}, 1488 cm^{-1}, and 1434 cm^{-1}, assigned to COO^- species, showed significant enhancement. Beyond 3 min of adsorption time, the appearance of the hydrogen band species at 3440 cm^{-1} indicated the involvement of hydroxyl groups in the adsorption process. The CO_2 adsorption process on the NH2-BX-SBA-15 sample, depicted in Fig. 8, involves initial physical adsorption, leading to the generation of ammonium-carbamate zwitterions. Subsequent deprotonation of these intermediates results in the dominance of adsorption products consisting of ammonium carbamate ion pairs. Notably, the participation of silicon hydroxyl groups on the material surface in the CO_2 capture process is evident, suggesting the possible presence of hydrogen-bonded ammonium carbamate ion pairs in the final product [51], alongside silylpropylcarbamate and hydrogen-bonded carbamic acid formations.

4. Conclusion

Acid treatment removes boron atoms to create more sites for silanol nest in SBA-15 was significantly enhancing silanol density. CO_2 capture capacity of the material was linearly related to the amine loading capacity, which is further determined by the amount of silanol groups. Excessive boron removal will lead to SBA-15 structure collapse and NH2-B10-SBA-15-AT exhibited the best capture performance in the DAC experiment. The stability of NH2-B10-SBA15-AT was validated by multiple adsorption and desorption tests. *In situ*-DRIFTS results indicated CO_2 was first physically adsorbed on the surface of the material. The ammonium carbamate ions were formed, followed by the carbamic acid (hydrogen-bonded) and silylpropylcarbamate were formed. All these results provide a guideline for the development of DAC materials.

CRediT authorship contribution statement

Hao Yuan: Data curation, Methodology, Writing – original draft, Writing – review & editing. **Peng Li:** Data curation, Methodology. **Xiali Sun:** Data curation, Methodology. **Dingli Cen:** Data curation. **Decun Luo:** Methodology. **Xianghui Yan:** Supervision. **Guangping Lei:** Supervision. **Wentao Zheng:** Supervision. **Zhun Hu:** Supervision, Writing – review & editing. **Ralph T. Yang:** Conceptualization, Supervision, Writing – review & editing.

Declaration of competing interest

The authors declare that they have no known competing financial interests or personal relationships that could have appeared to influence the work reported in this paper.

Data availability

Data will be made available on request.

Acknowledgements

The authors acknowledge the financial support from National Key Research and Development Program of China (Grant Number: 2022YFA1604104), Innovation Capability Support Program of Shaanxi (NO. 2023-CX-TD-26). The authors would like to thank Menghan Sun from Shiyanjia Lab (www.shiyanjia.com) for the ICP-OES analysis.

Appendix A. Supplementary data

Supplementary data to this article can be found online at https://doi.org/10.1016/j.seppur.2024.126720.

References

[1] H. Lee, K. Calvin, D. Dasgupta, G. Krinner, A. Mukherji, P.W. Thorne, C. Trisos, J. Romero, e.a. Aldunce, (2023).
[2] N. McQueen, K.V. Gomes, C. McCormick, K. Blumanthal, M. Pisciotta, J. Wilcox, A review of direct air capture (DAC): scaling up commercial technologies and innovating for the future, Progress in Energy 3 (2021).
[3] X. Zhu, W. Xie, J. Wu, Y. Miao, C. Xiang, C. Chen, B. Ge, Z. Gan, F. Yang, M. Zhang, D. O'Hare, J. Li, T. Ge, R. Wang, Recent advances in direct air capture by adsorption, Chem. Soc. Rev. 51 (2022) 6574–6651.
[4] X. Shi, H. Xiao, H. Azarabadi, J. Song, X. Wu, X. Chen, K.S. Lackner, Sorbents for the Direct Capture of CO2 from Ambient Air, Angew. Chem. Int. Ed. 59 (2020) 6984–7006.
[5] E.S. Sanz-Pérez, C.R. Murdock, S.A. Didas, C.W. Jones, Direct Capture of CO2 from Ambient Air, Chem. Rev. 116 (2016) 11840–11876.
[6] V. Nikulshina, M.E. Gálvez, A. Steinfeld, Kinetic analysis of the carbonation reactions for the capture of CO2 from air via the Ca(OH)2–CaCO3–CaO solar thermochemical cycle, Chem. Eng. J. 129 (2007) 75–83.

[7] J.K. Stolaroff, D.W. Keith, G.V. Lowry, Carbon Dioxide Capture from Atmospheric Air Using Sodium Hydroxide Spray, Environ. Sci. Tech. 42 (2008) 2728–2735.
[8] N.H. Florin, J. Blamey, P.S. Fennell, Synthetic CaO-Based Sorbent for CO2 Capture from Large-Point Sources, Energy Fuel 24 (2010) 4598–4604.
[9] B. Feng, H. An, E. Tan, Screening of CO2 Adsorbing Materials for Zero Emission Power Generation Systems, Energy Fuel 21 (2007) 426–434.
[10] W. Rahmah, G.T.M. Kadja, M.H. Mahyuddin, A.G. Saputro, H.K. Dipojono, I. G. Wenten, Small-pore zeolite and zeotype membranes for CO2 capture and sequestration – A review, J. Environ. Chem. Eng. 10 (2022).
[11] D. Fu, M.E. Davis, Carbon dioxide capture with zeotype materials, Chem. Soc. Rev. 51 (2022) 9340–9370.
[12] K.-M. Lee, Y.-H. Lim, C.-J. Park, Y.-M. Jo, Adsorption of Low-Level CO2 Using Modified Zeolites and Activated Carbon, Ind. Eng. Chem. Res. 51 (2012) 1355–1363.
[13] E. Pérez-Botella, S. Valencia, F. Rey, Zeolites in Adsorption Processes: State of the Art and Future Prospects, Chem. Rev. 122 (2022) 17647–17695.
[14] R.A. Khatri, S.S.C. Chuang, Y. Soong, M. Gray, Thermal and Chemical Stability of Regenerable Solid Amine Sorbent for CO2 Capture, Energy Fuel 20 (2006) 1514–1520.
[15] J. Wang, R. Fu, S. Wen, P. Ning, M.H. Helal, M.A. Salem, B.B. Xu, Z.M. El-Bahy, M. Huang, Z. Guo, L. Huang, Q. Wang, Progress and current challenges for CO2 capture materials from ambient air, Advanced Composites and Hybrid Materials 5 (2022) 2721–2759.
[16] L. Wang, R.T. Yang, Increasing Selective CO2 Adsorption on Amine-Grafted SBA-15 by Increasing Silanol Density, J. Phys. Chem. C 115 (2011) 21264–21272.
[17] A. Sayari, Y. Belmabkhout, Stabilization of Amine-Containing CO2 Adsorbents: Dramatic Effect of Water Vapor, J. Am. Chem. Soc. 132 (2010) 6312–6314.
[18] J.-T. Anyanwu, Y. Wang, R.T. Yang, CO2 capture (including direct air capture) and natural gas desulfurization of amine-grafted hierarchical bimodal silica, Chem. Eng. J. 427 (2022).
[19] L.T. Zhuravlev, The surface chemistry of amorphous silica, Zhuravlev Model, Colloids and Surfaces a: Physicochemical and Engineering Aspects 173 (2000) 1–38.
[20] H. Ghaedi, M. Zhao, Review on Template Removal Techniques for Synthesis of Mesoporous Silica Materials, Energy Fuel 36 (2022) 2424–2446.
[21] S.G. de Ávila, L.C.C. Silva, J.R. Matos, Optimisation of SBA-15 properties using Soxhlet solvent extraction for template removal, Microporous Mesoporous Mater. 234 (2016) 277–286.
[22] T.-L. Lai, Y.-Y. Shu, Y.-C. Lin, W.-N. Chen, C.-B. Wang, Rapid removal of organic template from SBA-15 with microwave assisted extraction, Mater. Lett. 63 (2009) 1693–1695.
[23] C. Pirez, K. Wilson, A.F. Lee, An energy-efficient route to the rapid synthesis of organically-modified SBA-15 via ultrasonic template removal, Green Chem. 16 (2014) 197–202.
[24] A.M. Norton, D. Kim, W. Zheng, N. Akter, Y. Xu, S.A. Tenney, D.G. Vlachos, M. Tsapatsis, J.A. Boscoboinik, Reversible Formation of Silanol Groups in Two-Dimensional Siliceous Nanomaterials under Mild Hydrothermal Conditions, J. Phys. Chem. C 124 (2020) 18045–18053.
[25] I.J. Pérez-Hermosillo, R. Ojeda-López, A. Domínguez-Ortiz, J. Marcos Esparza-Schulz, Hydrothermal rehydroxylation of SBA-15 material: Effect of initial silanol concentration and pore size on the textural properties, Materialia 28 (2023).
[26] I. Eswaramoorthi, A.K. Dalai, Synthesis, characterisation and catalytic performance of boron substituted SBA-15 molecular sieves, Microporous Mesoporous Mater. 93 (2006) 1–11.
[27] R. van Grieken, J.M. Escola, J. Moreno, R. Rodríguez, Direct synthesis of mesoporous M-SBA-15 (M=Al, Fe, B, Cr) and application to 1-hexene oligomerization, Chem. Eng. J. 155 (2009) 442–450.
[28] Y. Kuwahara, D.Y. Kang, J.R. Copeland, P. Bollini, C. Sievers, T. Kamegawa, H. Yamashita, C.W. Jones, Enhanced CO2 Adsorption over Polymeric Amines Supported on Heteroatom-Incorporated SBA-15 Silica: Impact of Heteroatom Type and Loading on Sorbent Structure and Adsorption Performance, Chemistry – A, European Journal 18 (2012) 16649–16664.
[29] Y. Wang, J.-T. Anyanwu, Z. Hu, R.T. Yang, Significantly enhancing CO2 adsorption on Amine-Grafted SBA-15 by boron doping and acid treatment for direct air capture, Sep. Purif. Technol. 309 (2023).
[30] D. Zhao, J. Feng, Q. Huo, N. Melosh, G.H. Fredrickson, B.F. Chmelka, G.D. Stucky, Triblock Copolymer Syntheses of Mesoporous Silica with Periodic 50 to 300 Angstrom Pores, Science 279 (1998) 548–552.
[31] D. Zhao, Q. Huo, J. Feng, B.F. Chmelka, G.D. Stucky, Nonionic Triblock and Star Diblock Copolymer and Oligomeric Surfactant Syntheses of Highly Ordered, Hydrothermally Stable, Mesoporous Silica Structures, J. Am. Chem. Soc. 120 (1998) 6024–6036.
[32] M. Thommes, K. Kaneko, A.V. Neimark, J.P. Olivier, F. Rodriguez-Reinoso, J. Rouquerol, K.S.W. Sing, Physisorption of gases, with special reference to the evaluation of surface area and pore size distribution (IUPAC Technical Report), Pure Appl. Chem. 87 (2015) 1051–1069.
[33] K. Miyazawa, S. Inagaki, Control of the microporosity within the pore walls of ordered mesoporous silica SBA-15, Chem. Commun. (2000) 2121–2122.
[34] R. Ryoo, C.H. Ko, M. Kruk, V. Antochshuk, M. Jaroniec, Block-Copolymer-Templated Ordered Mesoporous Silica: Array of Uniform Mesopores or Mesopore−Micropore Network? J. Phys. Chem. B 104 (2000) 11465–11471.
[35] D.-G. Choi, S.-M. Yang, Effect of two-step sol–gel reaction on the mesoporous silica structure, J. Colloid Interface Sci. 261 (2003) 127–132.
[36] P. Schmidt-Winkel, P. Yang, D.I. Margolese, B.F. Chmelka, G.D. Stucky, Fluoride-Induced Hierarchical Ordering of Mesoporous Silica in Aqueous Acid-Syntheses, Adv. Mater. 11 (1999) 303–307.
[37] A. Katiyar, S. Yadav, P.G. Smirniotis, N.G. Pinto, Synthesis of ordered large pore SBA-15 spherical particles for adsorption of biomolecules, J. Chromatogr. A 1122 (2006) 13–20.
[38] D. Zhao.Y. Wan.W. Zhou, Ordered Mesoporous Materials (2013) 153–217.
[39] P.I. Ravikovitch, A.V. Neimark, Characterization of Micro- and Mesoporosity in SBA-15 Materials from Adsorption Data by the NLDFT Method, J. Phys. Chem. B 105 (2001) 6817–6823.
[40] E.B. Celer, M. Jaroniec, Temperature-Programmed Microwave-Assisted Synthesis of SBA-15 Ordered Mesoporous Silica, J. Am. Chem. Soc. 128 (2006) 14408–14414.
[41] B. Aziz, N. Hedin, Z. Bacsik, Quantification of chemisorption and physisorption of carbon dioxide on porous silica modified by propylamines: Effect of amine density, Microporous Mesoporous Mater. 159 (2012) 42–49.
[42] M.-H. Yuan, L. Wang, R.T. Yang, Glow Discharge Plasma-Assisted Template Removal of SBA-15 at Ambient Temperature for High Surface Area, High Silanol Density, and Enhanced CO2 Adsorption Capacity, Langmuir 30 (2014) 8124–8130.
[43] A.S. D'Souza, C.G. Pantano, Hydroxylation and Dehydroxylation Behavior of Silica Glass Fracture Surfaces, J. Am. Ceram. Soc. 85 (2002) 1499–1504.
[44] X. Wang, C. Song, Carbon Capture From Flue Gas and the Atmosphere: A Perspective, Front. Energy Res. 8 (2020).
[45] C.-H. Chen, D. Shimon, J.J. Lee, F. Mentink-Vigier, I. Hung, C. Sievers, C.W. Jones, S.E. Hayes, The "Missing" Bicarbonate in CO2 Chemisorption Reactions on Solid Amine Sorbents, J. Am. Chem. Soc. 140 (2018) 8648–8651.
[46] Z. Bacsik, N. Ahlsten, A. Ziadi, G. Zhao, A.E. Garcia-Bennett, B. Martín-Matute, N. Hedin, Mechanisms and Kinetics for Sorption of CO2 on Bicontinuous Mesoporous Silica Modified with n-Propylamine, Langmuir 27 (2011) 11118–11128.
[47] N. Hiyoshi, K. Yogo, T. Yashima, Adsorption characteristics of carbon dioxide on organically functionalized SBA-15, Microporous Mesoporous Mater. 84 (2005) 357–365.
[48] C. Knöfel, C. Martin, V. Hornebecq, P.L. Llewellyn, Study of Carbon Dioxide Adsorption on Mesoporous Aminopropylsilane-Functionalized Silica and Titania Combining Microcalorimetry and in Situ Infrared Spectroscopy, J. Phys. Chem. C 113 (2009) 21726–21734.
[49] A. Danon, P.C. Stair, E. Weitz, FTIR Study of CO2 Adsorption on Amine-Grafted SBA-15: Elucidation of Adsorbed Species, J. Phys. Chem. C 115 (2011) 11540–11549.
[50] J. Yu, S.S.C. Chuang, The Structure of Adsorbed Species on Immobilized Amines in CO2 Capture: An in Situ IR Study, Energy Fuel 30 (2016) 7579–7587.
[51] M. Cho, J. Park, C.T. Yavuz, Y. Jung, A catalytic role of surface silanol groups in CO2 capture on the amine-anchored silica support, PCCP 20 (2018) 12149–12156.
[52] U. Tumuluri, M. Isenberg, C.-S. Tan, S.S.C. Chuang, In Situ Infrared Study of the Effect of Amine Density on the Nature of Adsorbed CO2 on Amine-Functionalized Solid Sorbents, Langmuir 30 (2014) 7405–7413.
[53] W.C. Wilfong, C.S. Srikanth, S.S.C. Chuang, In Situ ATR and DRIFTS Studies of the Nature of Adsorbed CO2 on Tetraethylenepentamine Films, ACS Appl. Mater. Interfaces 6 (2014) 13617–13626.
[54] Z. Bacsik, R. Atluri, A.E. Garcia-Bennett, N. Hedin, Temperature-Induced Uptake of CO2 and Formation of Carbamates in Mesocaged Silica Modified with n-Propylamines, Langmuir 26 (2010) 10013–10024.
[55] G. Zhang, P. Zhao, L. Hao, Y. Xu, Amine-modified SBA-15(P): A promising adsorbent for CO2 capture, J. CO2 Util. 24 (2018) 22–33.